Dear Author,

Please, note that changes made to the HTML content will be added to the article before publication, but are not reflected in this PDF.

Note also that this file should not be used for submitting corrections.

Journal of Solid State Chemistry ∎ (∎∎∎∎) ∎∎∎–∎∎∎

Contents lists available at ScienceDirect

Journal of Solid State Chemistry

journal homepage: www.elsevier.com/locate/jssc

Understanding the formation and growth of Ag nanoparticles on silver chromate induced by electron irradiation in electron microscope: A combined experimental and theoretical study

Maria T. Fabbro [a,b], Lourdes Gracia [d], Gabriela S. Silva [a], Luís P.S. Santos [c], Juan Andrés [d], Eloisa Cordoncillo [b], E. Longo [e,*]

[a] Department of Chemistry, CDMF/INCTMN, São Carlos Federal University, P.O. Box 676, CEP 13565-905 São Carlos, SP, Brazil
[b] Department of Inorganic and Organic Chemistry, Universitat Jaume I, Campus del Riu Sec, E-12071 Castellón, Spain
[c] Department of Chemistry, INCTMN, Maranhão Federal Institute, CEP 65030-005 São Luís, MA, Brazil
[d] Department of Physic and Analytical Chemistry, Universitat Jaume I, Campus del Riu Sec, E-12071 Castellón, Spain
[e] Chemistry Institute, CDMF/INCTMN, Paulista State University, CEP 14800-900 Araraquara, SP, Brazil

ARTICLE INFO

Article history:
Received 18 December 2015
Received in revised form
30 March 2016
Accepted 31 March 2016

Keywords:
Ag_2CrO_4
Order-disorder effects
Electron beam irradiation
Density-functional-theory

ABSTRACT

Ag_2CrO_4 microcrystals were synthesized using the co-precipitation method. These microcrystals were characterized through X-ray diffraction (XRD) with Rietveld analysis, field-emission scanning electron microscopy (FE-SEM), transmission electron microscopy (TEM) with energy-dispersive spectroscopy (EDS), micro-Raman (MR). XRD patterns and Rietveld refinement data showed that the material exhibits an orthorhombic structure without any deleterious phases. FE-SEM and TEM micrographs revealed the morphology and the growth of Ag nanoparticles on Ag_2CrO_4 microcrystals during electron beam irradiation. These events were directly monitored in real-time. Their optical properties were investigated using ultraviolet-visible (UV–vis) diffuse reflectance spectroscopy that allowed the calculation of the optical band gap energy. Theoretical analyses based on the density functional theory level indicate that the incorporation of electrons is responsible for structural modifications and formation of defects on the $[AgO_6]$ and $[AgO_4]$ clusters, generating ideal conditions for the growth of Ag nanoparticles.

1. Introduction

Silver chromate, Ag_2CrO_4, exhibit an orthorhombic structure belonging to the space group *Pnma* at room temperature [1], the constituent clusters of this system are elongated (AgO_6) octahedral, distorted off-centered (AgO_4) tetrahedral, and (CrO_4) tetrahedral. The oxygen atoms are coordinated to the Ag atoms to generate a three-dimensional network [2]. In the electronic structure, the upper portion of the valence band (VB) is raised by the hybridization of Ag 4d and O 2p orbitals, while the position of the conduction band (CB) bottom controls the antibonding interaction between the Cr 3d and O 2p orbitals, resulting in a narrow band gap of ~1.80 eV [3]. This low value can enable strong absorption in the visible spectrum [2], which might help in achieving excellent photocatalytic activity under visible light [2,4–6].

Recent advances in *in situ* electron microscopy techniques have allowed direct observation of an interesting behavior of silver compounds, such as α-Ag_2WO_4, i.e. by exposure to electron beams of an electronic microscope and under high vacuum. These compounds undergo in situ nucleation of Ag nanofilaments on the α-Ag_2WO_4 surface [7–9] and in this study, we have elucidated nonclassical growth mechanisms of Ag. Nevertheless, similar phenomena take place in β-Ag_2MoO_4 [10], and Ag_3PO_4 crystals [11].

In this paper, we present a combination of experimental and theoretical studies devoted to rationalizing early events associated with the formation of Ag nanoparticles on Ag_2CrO_4. First, we synthesized this material using the co-precipitation method, and their crystal structure were characterized through experimental techniques, such as X-ray diffraction (XRD) with Rietveld analysis, field-emission scanning electron microscopy (FE-SEM), transmission electron microscopy (TEM) with energy-dispersive spectroscopy (EDS), micro-Raman (MR) spectroscopy, and ultraviolet-visible (UV–vis) diffuse reflectance spectroscopy. Subsequently, we observed the electron-irradiation-induced formation of Ag nanoparticles on the Ag_2CrO_4 surface. To complement and rationalize experimental measurements, the quantum theory of atoms in molecules (QTAIM) developed by Bader and co-workers [12–14] was used in order to obtain a mechanism capable of explaining the electron redistribution induced by the excess electrons in both the

* Corresponding author.
E-mail address: elson@iq.unesp.br (E. Longo).

http://dx.doi.org/10.1016/j.jssc.2016.03.050
0022-4596/

bulk and surface of Ag_2CrO_4. In addition, this theory was used to determine the relationship between the structural and electronic changes in both Ag-O and Cr-O bonds of the constituent clusters: (AgO_6), (AgO_4), and (CrO_4).

2. Experimental section

2.1. Synthesis of Ag_2CrO_4

Ag_2CrO_4 microcrystals were synthesized, without the use of a surfactant, via the co-precipitation method. For this synthesis, 50 mL of distilled water were added to 1×10^{-3} mol of $Na_2CrO_4 \cdot 2H_2O$ (99.5% pure, Alfa Aesar) and stirred at room temperature until total solution was obtained. Parallel to this process, 2×10^{-3} mol of $AgNO_3$ (99.8% pure, Alfa Aesar) were dissolved in 50 mL of distilled water. When both solutions turned homogeneous, both temperatures were increased to approximately 90 °C. A silver salt solution was then added to the chromate salt solution by means of a constant drip process, thereby leading to the formation of precipitates. This suspension was stirred at ~90 °C for 30 min. The precipitates were collected by centrifugation, washed several times with water and ethanol, and dried at 60 °C for 24 h.

2.2. Characterization

The Ag_2CrO_4 sample was structurally determined by XRD (DMax/2500 PC diffractometer, Rigaku) using monochromatized Cu-Kα radiation (λ=1.5406 Å). The diffraction pattern was performed in the Rietveld routine over 2θ range from 10 to 110° with a scanning velocity of 1° min^{-1}, and a scan step width of 0.02°. The phase analysis conducted via the Rietveld method [15] was performed by using the general structure analysis system (GSAS) software [16,17]. The shapes, sizes, visualization of the Ag nanoparticles and element distribution of the Ag_2CrO_4 microcrystals were observed by FE-SEM (Inspect F50, FEI) operated at 5 kV, and TEM operating at 200 kV and energy-dispersive spectroscopy (EDS) (Tecnai G2TF20, FEI). Furthermore, TEM images were obtained from samples prepared by drying droplets of the as-prepared samples from an acetone dispersion sonicated for 10 min, and then deposited on the Cu grids. MR measurements were conducted by using a modular Raman spectrometer (model RMS-550, Horiba, Jobin Yvon), with Ar–laser excitation at 514 nm, and a fiber-microscope operating at 400–1100 cm^{-1}.

2.3. Computational details

We have studied the geometric and electronic structure of Ag_2CrO_4, and have derived a mechanism sequence using electron irradiation as relevant to early events for the formation and growth of Ag filaments from AgO_6 and AgO_4 and CrO_4 clusters, as its constituent polyhedral. First-principles total-energy calculations were performed within the density-functional-theory (DFT) framework using the VASP program [18,19]. The Kohn-Sham equations were solved by means of the Perdew–Burke–Ernzerhof (PBE) exchange-correlation functional [20]. In addition, the electron-ion interaction was described by the projector-augmented-wave pseudopotentials [20,21]. The plane-wave expansion was truncated at a cut-off energy of 400 eV and the Brillouin zones were sampled through Monkhorst-Pack special k-point grids; these ensure the geometrical and energetic convergence for the Ag_2CrO_4 structures considered in this work. Vibrational-frequencies were calculated at the Γ point within the harmonic approximation, and the dynamical matrix was computed via numerical evaluation of the first-derivative of the analytical atomic gradients. Furthermore, as increase the number of electrons in the bulk structure was increased, and the volume of the unit-cell and the atomic positions of all the crystal structures were optimized simultaneously. Bader [12, 22] determined the relationship between the charge density topology and elements of molecular structure and bonding. This relationship, i.e., Bader's quantum theory of atoms in molecules (QTAIM) [12,14], is now a well-established tool used to analyze the electron density, describe interatomic interactions, and rationalize chemical bonding. Atomic charges were calculated using integrations of the charge density (n) within the atomic basins, Ω, and subtracting the nuclear charge, Z, of the corresponding atom.

$$q\,(\Omega) = Z_{\Omega} - n(\Omega) \text{ with } n\,(\Omega) = \int_{\Omega} \rho(\Omega) dr \quad (1)$$

The computations performed in this study can be very helpful achieving a thorough understanding of the distribution of excess electrons in this material; the relation between this distribution and the structural and electronic evolution is provided. Theoretical calculations are also used to determine the effect of electron irradiation on the strength of the Ag-O and Cr-O bonds. We will discuss the role of this analysis, performed on both experimental and theoretical results, in determining the structural and electronic structure of Ag_2CrO_4 and hence in explaining the Ag nucleation process.

3. Results and discussion

3.1. Rietveld refinement analyses

Fig. 1 depicts the observed, calculated and difference profiles in the 2θ range of 10–110° for Ag_2CrO_4 powder using orthorhombic space group *Pnma*. The fit between the observed and calculated profiles indicate that this material has an orthorhombic structure, without deleterious phases, in good agreement with the inorganic crystal structure database (ICSD) Card no. 16298 [1]. In addition, the well-defined peaks are indicative of long-range structural order and a high level of crystallinity. This refinement was performed by using the general structure analysis (GSAS) program

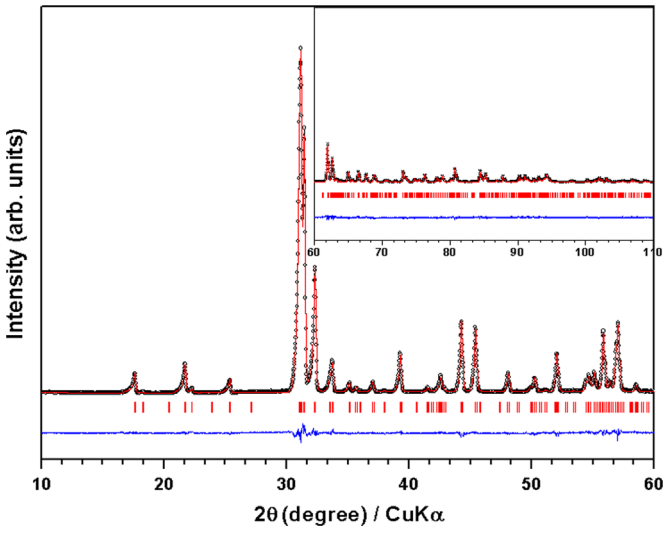

Fig. 1. Observed (black circles), calculated (red line), and difference (blue line below) profiles obtained after Rietveld refinement for Ag_2CrO_4 using orthorhombic space group *Pnma*. The series of tick marks indicate the allowed Bragg positions. Inset shows the patterns in the 2θ range of 60–110°. (For interpretation of the references to color in this figure legend, the reader is referred to the web version of this article.)

Table 1
Refined structural parameters of Ag_2CrO_4 using orthorhombic space group *Pnma*.

Ions	Fractional coordinates			Thermal parameter
	X	Y	Z	B (Å^2)
Ag^{+1}	0.500000	0.500000	0.500000	0.02454
Ag^{+1}	0.134714	0.250000	0.499437	0.03446
Cr^{+6}	0.316477	0.250000	−0.012419	0.01470
O^{-2}	0.150245	0.250000	−0.069363	0.00563
O^{-2}	0.344487	0.250000	0.286966	0.02048
O^{-2}	0.388294	0.442817	−0.135797	0.03915

a=10.066747 (Å); b=7.025253 (Å); c=5.540493 (Å); V=391.832 (Å^3); R_{wp}=0.0855; R_p=0.0583; R_{Bragg}=0.0604; χ^2=2.101.

Table 2
Lattice parameters and cell volume of the Ag_2CrO_4 structure, showing theoretical and experimental values of this work and compared to other reported data.

	Theor	Exp	Exp [26]	Theor [26]
a (Å)	10.176	10.066	10.065 (4)	10.224
b (Å)	7.011	7.025	7.013 (3)	7.025
c (Å)	5.618	5.540	5.538 (2)	5.653
V (Å^3)	400.73	391.83	390.9 (4)	406.02

[16,17]. The refined structural parameters and various agreement factors are given in Table 1.

Q4 The theoretical (DFT calculations) estimated values of the lattice parameters of the Ag_2CrO_4 structure concur with those obtained via Rietveld refinement are summarized in Table 2. Others theoretical and experimental data have been collected in Table 2 for comparison purposes.

3.2. UV–vis absorption spectroscopy and DOS analysis

The optical band gap energy (E_{gap}) was determined by using the method proposed by Kubelka and Munk [23]. This methodology is based on the transformation of diffuse reflectance measurements to estimate E_{gap} values with good accuracy within the limits of assumptions when modeled in three dimensions [24]. The Kubelka-Munk Eq. (2) for any wavelength is given as:

$$F(R_\infty)=\frac{(1-R_\infty)^2}{2R_\infty}=\frac{k}{s} \quad (2)$$

where $F(R_\infty)$ is the Kubelka–Munk function or absolute reflectance of the sample. In that case, magnesium oxide (MgO) was used as the standard sample in the reflectance measurements. In Eq. (2), $R_\infty=R_{sample}/R_{MgO}$ (R_∞ is the reflectance of an infinitely thick sample), k is the molar absorption coefficient, and s is the scattering coefficient. The optical band gap and absorption coefficient of semiconductor oxides [2] that have a parabolic band structure, are calculated by using the following equation:

$$\alpha h\nu=C_1(h\nu-E_{gap})^n \quad (3)$$

where α is the linear absorption coefficient of the material, $h\nu$ is the photon energy, C_1 is a proportionality constant, E_{gap} is the optical gap, and n is a constant associated with the different types of electronic transitions, $n=0.5$ (direct allowed), $n=1.5$ (direct forbidden), $n=2$ (indirect allowed), and $n=3$ (indirect forbidden), respectively. Xu et al. [3] reported that the silver chromate crystals exhibited an optical absorption spectrum governed by indirectly allowed electronic transitions between the valence and conduction bands. Therefore, in this work, a value of $n=2$ was used in Eq. (3). Finally, using the remission function described in Eq. (2) and with the term k=2α and C_2 is proportionality constant, we obtain the modified Kubelka–Munk equation that is given as follows:

$$[F(R_\infty)h\nu]^2=C_1(h\nu-E_{gap}) \quad (4)$$

1.70 eV was determined from the plot of $[F(R_\infty)h\nu]^2$ against $h\nu$ (Fig. 2a) of the Ag_2CrO_4 crystals.

The computed band structure and total DOS projected onto the atoms and orbitals of the Ag_2CrO_4 structure are shown in Fig. 2b, in order to facilitate the comparison between the theoretical and experimental results. Indirect and direct band gap values of 1.37 eV (from Γ to T) and 1.51 eV (from Γ to Γ), respectively, are obtained from the calculations. This difference is attributed primarily to the distortions on both the $[AgO_y]$ (y=6, or 4) and $[CrO_4]$ clusters at short and medium-range. An analysis of the projected DOS reveals that the top of the VB is formed mainly by the hybridization between the Ag *4d* and O *2p* orbitals; however, the bottom of the CB is formed mainly by the hybridization between the Cr *3d* and O *2p* orbitals. The major contribution to the maximum of VB is produced by O *2p* and Ag $4d_{z^2}$, $4d_{xz}$ and $4d_{xy}$ states, showing an overlap between O 2*p* and Ag 4*d* orbitals stronger than that between O 2*p* and 3*d* Cr ones. Besides, the bottom of CB is derived mostly from Cr *3dxz* states and Ag *5s* states in minor extent, with its bottom located at *T*-point of the Brillouin path.

3.3. Raman scattering analyses

Raman spectroscopy is considered a powerful technique to estimate the local structural order or short-range order of solids. According to group-theory analysis, the allowed representation for each Wyckoff position of the Ag_2CrO_4 structure, described by the *Pnma* space group, exhibits 36 Raman-active modes. These modes correspond to the decomposition at the Γ point (i.e., $\Gamma=11A_g+7B_{1g}+7B_{3g}+11B_{2g}$). The most intense peaks and considerably weaker ones occur at wavenumbers of 750–900 cm^{-1} and 350–450 cm^{-1} in the high- and medium-frequency regions, respectively. These peaks correspond to the respective stretching and bending modes of the CrO_4 group, as previously reported in the literature [25–27]. The spectrum collected from the Ag_2CrO_4 (Fig. 3) exhibits broad vibrational modes, which are indicative of short-range structural disorder. Furthermore, the most intense peaks occur in the high-frequency region, at 780–816 cm^{-1}, and are attributed to the symmetric stretching vibrations of Cr-O bond in the $[CrO_4]$ clusters (A_g mode). Small shifts in the Raman mode positions arise from various factors such as the preparation method, average crystal size, interaction forces between the ions, or the degree of structural order in the lattice. The modes in the region between 350 and 450 cm^{-1} that were not experimentally observed were predicted by the first-principles calculation, suggesting that their intensity may be low in the Raman spectra.

3.4. FE-SEM image analyses

Fig. 4(a.1–6 and b.1–6) shows a time-resolved series of FE-SEM images obtained under high vacuum (1×10^{-5} Pa) during the growth of Ag nanoparticles after the absorption of energetic electrons on the Ag_2CrO_4 surface at different times: 0–5 min. Fig. 4 (c.1–6) also shows the size distribution of Ag nanoparticles after 5 min of image acquisition. As observed in Fig. 4, when the absorption of energetic electrons by the Ag_2CrO_4 surface occurs, the nucleation of Ag nanoparticles generating Ag vacancy defects occurs, which are related to the different average size distributions of particles. The formation of Ag nanoparticles continues as the exposure time increases. However, the growth process does not have a preferred region but rather occurs in all regions irradiated by the electron beam.

Please cite this article as: M.T. Fabbro, et al., J. Solid State Chem. (2016), http://dx.doi.org/10.1016/j.jssc.2016.03.050

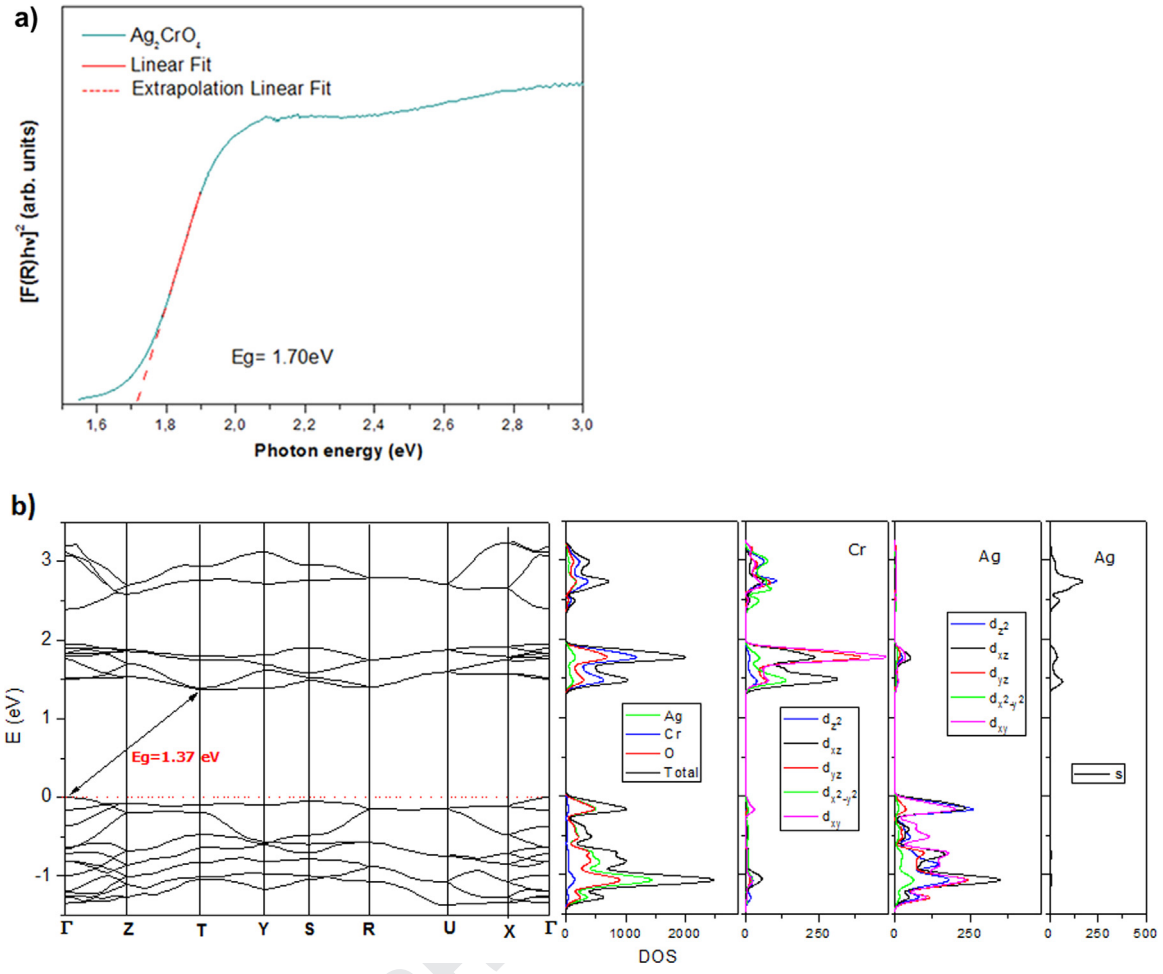

Fig. 2. (a) UV–vis spectra of the Ag_2CrO_4. (b) Theoretical band structure and density of states projected onto the atoms and orbitals. The Fermi energy is set at 0 eV as reference.

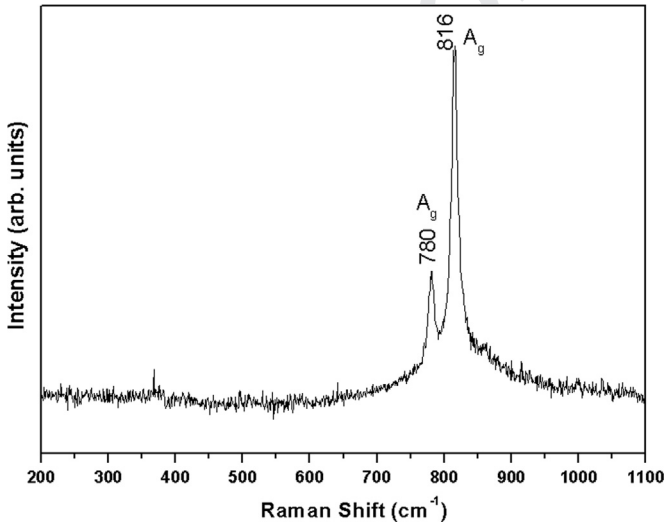

Fig. 3. Raman scattering spectrum of the Ag_2CrO_4.

3.5. TEM image and EDS pattern analyses

Proving the Ag nanoparticles growth on the material surface, Fig. 5 shows the TEM images and EDS characterization of Ag_2CrO_4 and the composition of Ag, Cr and O in the sample. Point 1, which is located in the Ag filament, has a Ag content of 100% Ag. Point 2, which is located in the vicinity of the interface, is composed of ~83.92% Ag, 14.64% O, and 1.42% Cr. However, points 3 and 4, which are located in the internal region of the Ag_2CrO_4, are composed of 78.25% Ag, 6.76% O, 14.98% Cr, and 78.42%Ag, 6.01% O, and 15.57% Cr, respectively.

The electron beam irradiation leads to the formation of defects, such as Ag vacancies (V'_{Ag}) or oxygen vacancies ($V_{\dot{O}}$ or $V_{\ddot{O}}$) in the Ag_2CrO_4 microcrystals. The electron absorption effect on the crystal surface generates an n-type semiconductor with Ag vacancies, described by equations as follows:

$$[AgO_y]^x + \left[AgO_{y-1}V_{\dot{O}}^{\times}\right] \rightarrow [AgO_y]' + \left[AgO_{y-1}V_{\dot{O}}\right] \quad (5)$$

$$[AgO_y]^x + e' \rightarrow [V'_{Ag}O_y]^x + Ag^0 \quad (6)$$

The formation of Ag^0 promotes Ag-nanoparticle growth on the surface of the Ag_2CrO_4 microcrystal. According to (Eqs. (5) and 6), the microcrystal is an n-type semiconductor characterized by the oxygen vacancies. Electron irradiation of the material induces the formation of Ag vacancies, and thereby transforms the specific region to a p-type semiconductor. In fact, the size of the Ag nanoparticles increases with increasing concentration of Ag vacancies. The material is therefore transformed from an n-type semiconductor to an n-type semiconductor with p-type semiconductor in specific regions, owing to the electron-induced formation of internal defects. This formation and the corresponding structural modifications of the [AgO_6] and [AgO_4] clusters are confirmed via the theoretical analysis.

Please cite this article as: M.T. Fabbro, et al., J. Solid State Chem. (2016), http://dx.doi.org/10.1016/j.jssc.2016.03.050

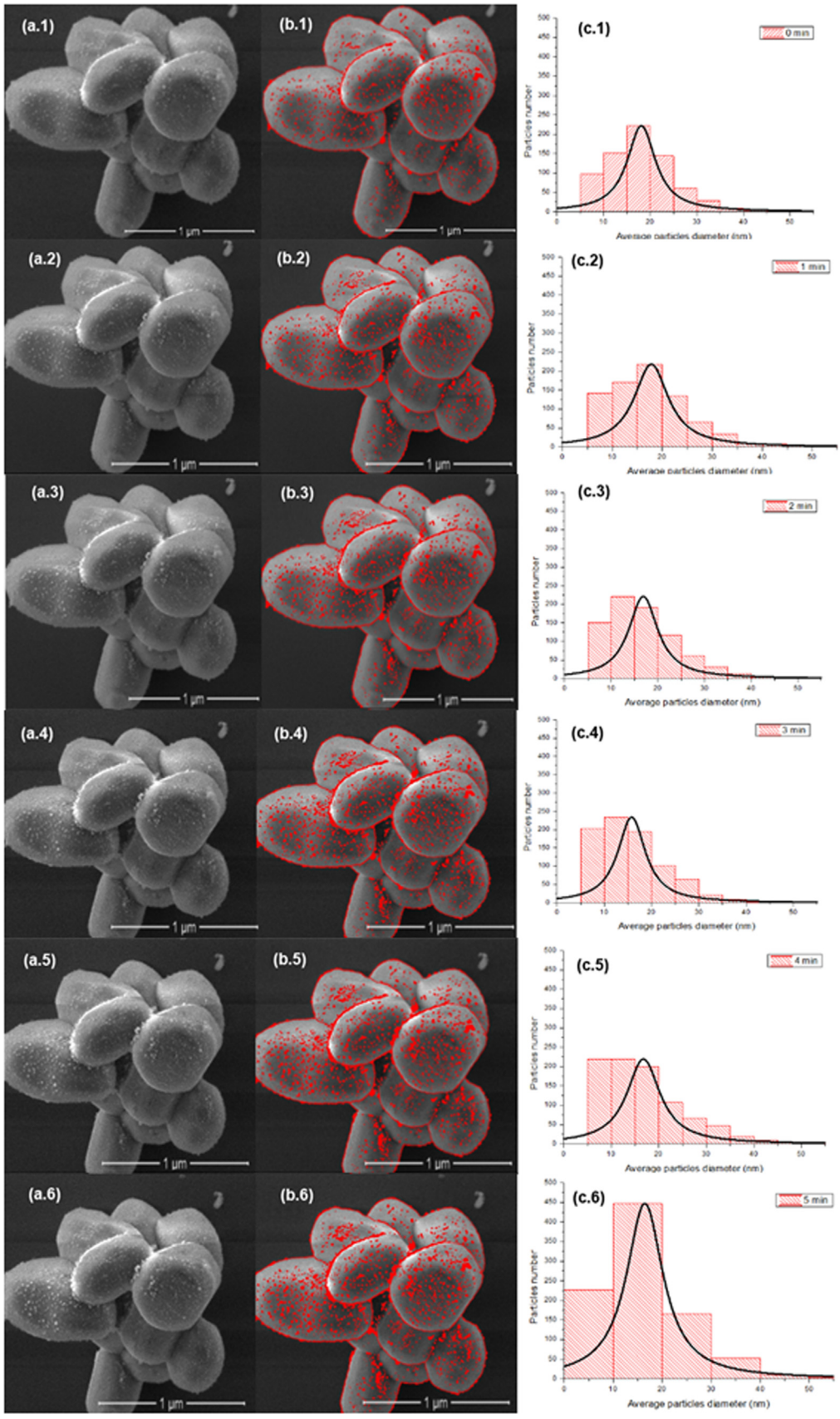

Fig. 4. FE-SEM images of the Ag_2CrO_4 microcrystals (left) and growth of the Ag nanoparticles on the Ag_2CrO_4 surface at 0, 1, 2, 3, 4, and 5 min (right), respectively; histograms of Ag particle size distribution at different times.

Please cite this article as: M.T. Fabbro, et al., J. Solid State Chem. (2016), http://dx.doi.org/10.1016/j.jssc.2016.03.050

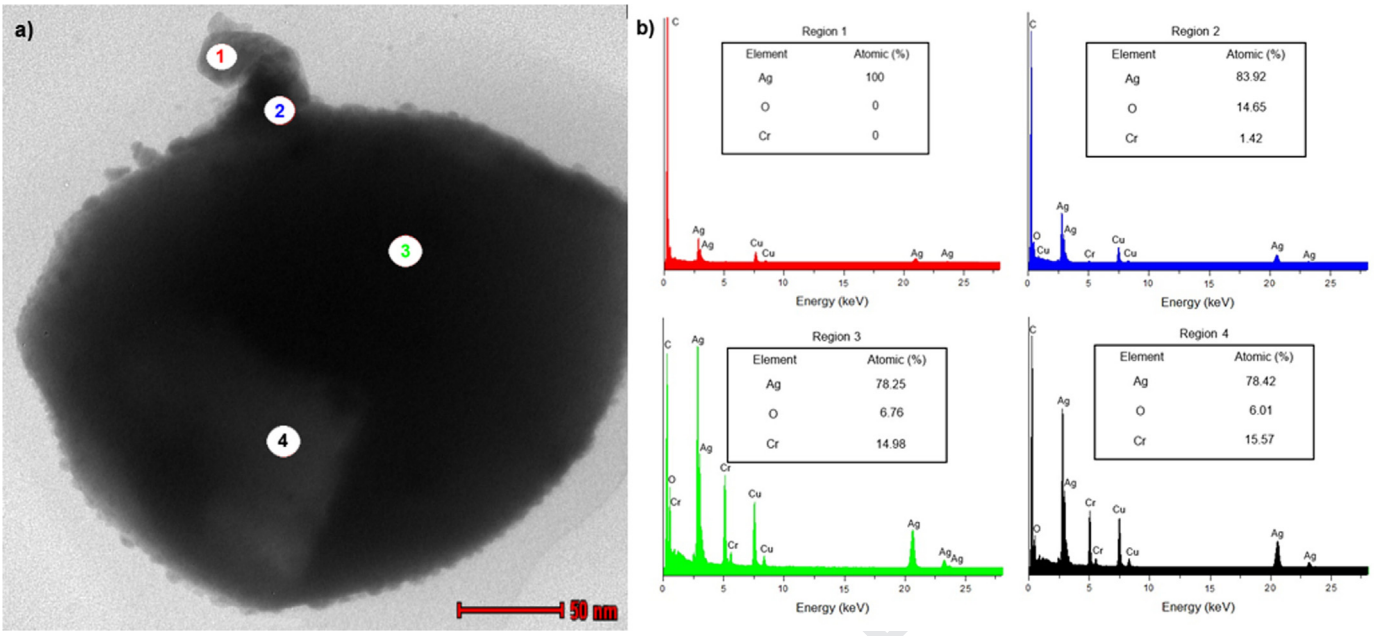

Fig. 5. (a) TEM image of the Ag_2CrO_4, and (b) EDS spectra controlled form four regions.

3.6. Electronic structure analysis

In light of the experimental results shown in Figs. 4 and 5, theoretical calculations were performed in order to understand the phenomenon of electron absorption that leads to the growth of Ag nanostructures. A maximum of seven electrons were introduced into the octahedral [AgO_6] and tetrahedral [AgO_4] and [CrO_4] clusters of the orthorhombic Ag_2CrO_4 structure (see Fig. 6).

The theoretically estimated values of the lattice parameters, and bond lengths as a function of the number of electrons (N) are shown in Table 3. As the table shows, the lattice parameters and the lengths of the Ag1-O and Ag2-O bonds increase significantly with increasing number of electrons; however, the opposite trend is observed in the case of the Ag1-Ag2 bond.

For N=3, [AgO_6] transforms to [AgO_4]′, and [AgO_4] is maintained. When one more electron is added (N=4), [AgO_4]′ transforms to [AgO_2], and Ag1 is coordinated to two O atoms at 2.27 Å. On the other hand, Ag2, which forms [AgO_4] clusters, maintains its coordination with three equal distances at 2.50 Å, until N=6. When the addition of five electrons was taken into account in the calculations, the Ag1-Ag2 distance decreased from more than 3–2.92 Å, 2.78 Å, and 2.75 Å at N=5, N=6, and N=7, respectively.

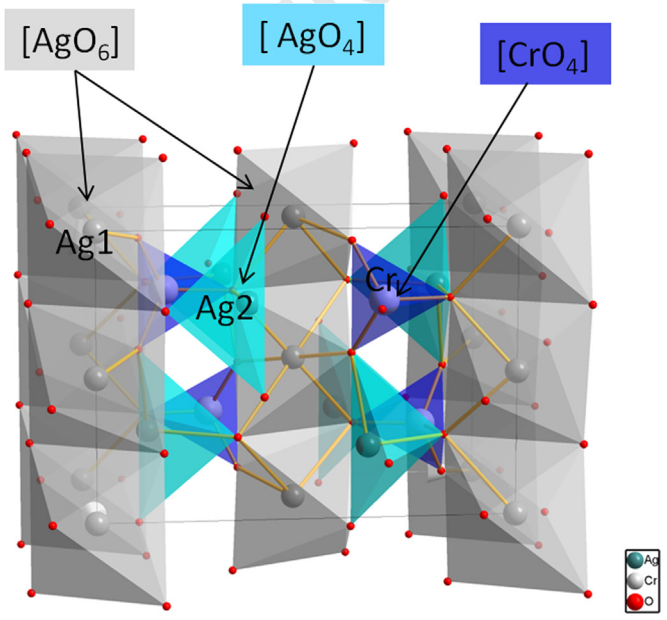

Fig. 6. Theoretical representation of the Ag_2CrO_4 orthorhombic structure.

Table 3
Lattice parameter and bond length as a function of the number of electrons (N) added. Three different sets of values are shown for the bond lengths: two sets of equal values for the Ag1-O distance and one for the Ag2-O distance.

N	Cell parameters (Å)			Bond lengths (Å)		
	a	b	c	Ag1-O in [AgO_6]	Ag2-O in [AgO_4]	Ag1-Ag2
0	10.176	7.011	5.618	2.32, 2.40, 2.67	2.31, 2.39, 2.45	3.59
1	10.405	7.079	5.676	2.35, 2.45, 2.73	2.33, 2.41, 2.49	3.62
2	10.751	7.172	5.747	2.27, 2.63, 2.89	2.36, 2.38, 2.48	3.60
3	11.131	7.282	5.933	2.16, 2.94, –	2.40, 2.35, 2.40	3.55
4	11.297	7.463	6.104	2.27	2.37, 2.55, 2.48	3.28
5	11.457	7.644	6.116	2.30	2.44, 2.95, 2.60	2.92
6	11.696	7.533	6.354	2.75	2.51, – , 2.50	2.78
7	13.538	7.612	7.247	2.88	2.71, – , 2.64	2.75

The four Cr-O bond lengths remain practically constant as the number of electrons is increased. Hence, the theoretical analyses indicate the incorporation of electrons is responsible for structural modifications and formation of defects on the [AgO_6] and [AgO_4] clusters, generating the ideal conditions for the growth of Ag nanoparticles.

The Bader charge density of Ag, Cr and O centers as a function of N is presented in Fig. 7. Theoretical calculations indicate that Ag atoms of [AgO_6] and [AgO_4] clusters have a higher tendency to be reduced rather than the Cr atoms. Particularly at N=6, Ag1 and Ag2 atoms are practically reduced (from 0.81e to 0.01e) and almost reduced (from 0.74e to 0.14e), whereas for Cr atoms a constant value of the electron density is maintained (slight decrease of 0.25 units at N=7).

An analysis of the results presented in Table 3 and Fig. 7 reveals that the electron density distribution is enhanced between Ag1–Ag2 at the same time that the Ag1–Ag2 contact distance is significantly shortened when the number of added electrons is up to

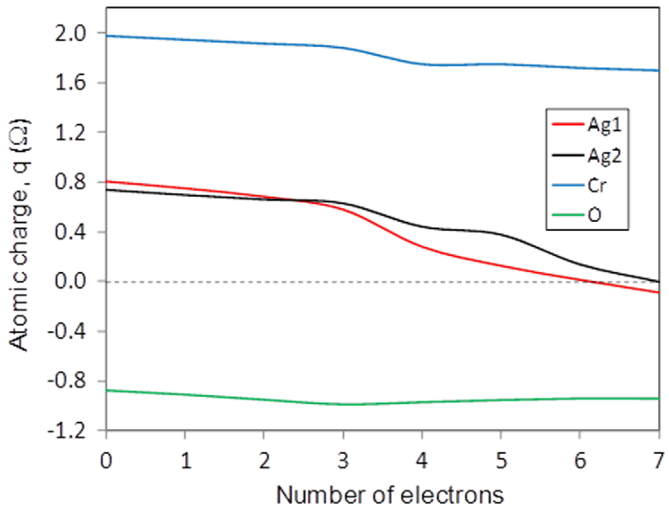

Fig. 7. The Bader charge density of Ag, Cr and O centers as a function of *N*.

4. In addition, there is an electronic charge density enlargement in the vicinity of Ag1 from N=4 since Ag1 is coordinated to only two O atoms, being more prone to reduction than Ag2 atoms. At N=6, the Ag1 atoms are practically reduced, whereas the Ag2 atoms require 7 electrons to reach the same state. This behavior implies the existence of two different paths to obtaining metallic Ag, which are associated with the $[AgO_2]$ (coming from $[AgO_6]$) and $[AgO_4]$ clusters.

Two-dimensional charge density maps associated with the interaction of $[AgO_6]$ clusters and $[AgO_6]$–$[AgO_4]$ clusters are presented in Fig. 8a and b, respectively. Fig. 8a shows charge density maps associated with four Ag1–O bonds of $[AgO_6]$ clusters, considering a neutral state (N=0) and addition of three (N=3) and six (N=6) electrons, respectively. The zones with high and low charge densities are specified by the concentration of charge lines around the atoms, revealing a decrease in the electronic charge density between Ag and O atoms for N from 0 to 6. Thus, the Ag-O bond lengths are enlarged because of the perturbation caused in the system with the incorporation of electrons (N=6). In addition, the charge density maps presented in Fig. 8b indicates that the interactions of $[AgO_6]$ and $[AgO_4]$ clusters also become weaker when N is increased from 0 to 6, in good agreement with the shortening of Ag1–Ag2 distances presented in Table 3. Hence, both behaviors theoretically obtained in the Fig. 8a and b can be associated with the growth of metallic Ag nanoparticles.

Consequently, the electron excess imposed in the material is transferred from one cluster to another through the Ag_2CrO_4 lattice, so that the formation and growth processes of Ag involve adjacent $[AgO_6]$ and $[AgO_4]$ clusters.

4. Conclusion

In this work, we report the synthesis of Ag_2CrO_4 via a simple precipitation method and, the first-ever in situ formation and growth of Ag nanoparticles on the surface of the Ag_2CrO_4. The XRD pattern present that the silver chromate microcrystals have orthorhombic structure with a space group *Pnma* and well-defined diffraction peaks, which indicate a structural order and crystallinity at long range, confirmed by the Rietveld refinement data. The material also exhibited short range structural disorder, as indicating by the Raman-active mode. Moreover, the E_{gap} value, determined from UV–vis measurements, corresponded to the energy level between the VB and CB. The growth of the Ag-nanoparticles during electron beam irradiation, was monitored in real-

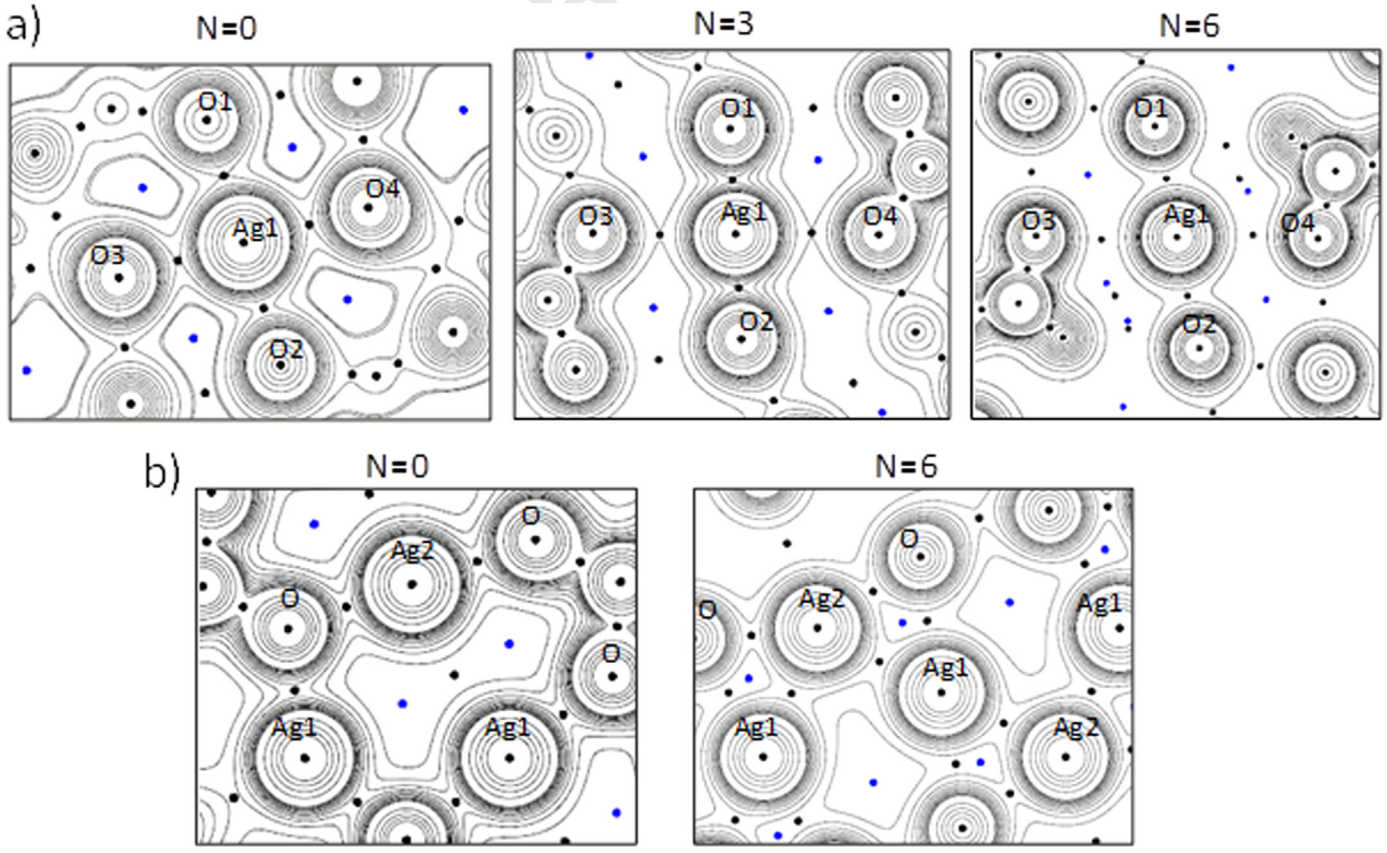

Fig. 8. Charge density maps associated with the interaction of (a) $[AgO_6]$ clusters, and (b) $[AgO_6]$ and $[AgO_4]$ clusters.

Please cite this article as: M.T. Fabbro, et al., J. Solid State Chem. (2016), http://dx.doi.org/10.1016/j.jssc.2016.03.050

time; the growth of the nanoparticles increased with increasing irradiation time. This growth was evaluated by using an FE-SEM and a TEM with EDS capabilities. In fact, these techniques were used to characterize the microcrystals and the Ag nanoparticles obtained.

Defects on the $[AgO_6]$ and $[AgO_4]$ clusters are generated by electron-induced modifications in the structure, and provide favorable conditions for the formation of Ag nanoparticles. In addition, these modifications in the interior material region under electron irradiation are capable of changing the n-type semiconductor to an n-type semiconductor with p-type semiconductor in specific regions. The results of theoretical calculations performed in this work, exhibit close correspondence to the Ag-nanoparticle growth observed experimentally.

Acknowledgments

The authors acknowledge the financial support of the following agencies: Conselho Nacional de Desenvolvimento Científico e Tecnológico: 237944/2012-0; Fundação de Amparo à Pesquisa do Estado de São Paulo: 2013/07296-2. Generalitat Valenciana for PrometeoII/2014/022 and ACOMP/2014/270, and Ministerio de Economia y Competitividad, project CTQ2012-36253-C03-02 and ACOMP/2014/270.

References

[1] M.L. Hackert, R.A. Jacobson, The crystal structure of silver chromate, J. Solid State Chem. 3 (1971) 364–368, http://dx.doi.org/10.1016/0022-4596(71)90072-7.

[2] S. Ouyang, Z. Li, Z. Ouyang, T. Yu, J. Ye, Z. Zou, Correlation of crystal structures, electronic structures, and photocatalytic properties in a series of Ag-based oxides: $AgAlO_2$, $AgCrO_2$, and Ag_2CrO_4, J. Phys. Chem. C 112 (2008) 3134–3141, http://dx.doi.org/10.1021/jp077127w.

[3] D. Xu, S. Cao, J. Zhang, B. Cheng, J. Yu, Effects of the preparation method on the structure and the visible-light photocatalytic activity of Ag_2CrO_4, Beilstein J. Nanotechnol. 5 (2014) 658–666, http://dx.doi.org/10.3762/bjnano.5.77.

[4] W. Zhao, Y. Guo, S. Wang, H. He, C. Sun, S. Yang, A novel ternary plasmonic photocatalyst: ultrathin g-C_3N_4 nanosheet hybrided by $Ag/AgVO_3$ nanoribbons with enhanced visible-light photocatalytic performance, Appl. Catal. B Environ. 165 (2015) 335–343, http://dx.doi.org/10.1016/j.apcatb.2014.10.016.

[5] Y. Liu, H. Yu, M. Cai, J. Sun, Microwave hydrothermal synthesis of Ag_2CrO_4 photocatalyst for fast degradation of PCP-Na under visible light irradiation, Catal. Commun. 26 (2012) 63–67, http://dx.doi.org/10.1016/j.catcom.2012.04.017.

[6] D. Xu, B. Cheng, S. Cao, J. Yu, Enhanced photocatalytic activity and stability of Z-scheme Ag_2CrO_4-GO composite photocatalysts for organic pollutant degradation, Appl. Catal. B Environ. 164 (2015) 380–388, http://dx.doi.org/10.1016/j.apcatb.2014.09.051.

[7] L.S. Cavalcante, M.A.P. Almeida, W. Avansi, R.L. Tranquilin, E. Longo, N. C. Batista, et al., Cluster coordination and photoluminescence properties of α-Ag_2WO_4 microcrystals, Inorg. Chem. 51 (2012) 10675–10687, http://dx.doi.org/10.1021/ic300948n.

[8] E. Long, , L.S. Cavalcante, D.P. Volanti, A.F. Gouveia, V.M. Longo, J.A. Varela, Direct in situ observation of the electron-driven synthesis of Ag filaments on α-Ag_2WO_4 crystals, Sci. Rep. 3 (2013) 1676, http://dx.doi.org/10.1038/srep01676.

[9] J. Andrés, L. Gracia, P. Gonzalez-Navarrete, V.M. Longo, W. Avansi, D.P. Volanti, et al., Structural and electronic analysis of the atomic scale nucleation of Ag on α-Ag_2WO_4 induced by electron irradiation, Sci. Rep. 4 (2014) 5391, http://dx.doi.org/10.1038/srep05391.

[10] J. Andrés, M.M. Ferrer, L. Gracia, A. Beltran, V.M. Longo, G.H. Cruvinel, et al., A Combined experimental and theoretical study on the formation of Ag filaments on β-Ag_2MoO_4 induced by electron irradiation, Part. Part. Syst. Charact. 32 (2015) 646–651, http://dx.doi.org/10.1002/ppsc.201400162.

[11] G. Botelho, J.C. Sczancoski, J. Andres, L. Gracia, E. Longo, Experimental and theoretical study on the structure, optical properties, and growth of metallic silver nanostructures in Ag_3PO_4, J. Phys. Chem. C 119 (2015) 6293–6306, http://dx.doi.org/10.1021/jp512111v.

[12] R.F.W. Bader, Atoms in Molecules: A Quantum Theory (International Series of Monographs on Chemistry), Clarendon Press, Oxford, New York, 1990.

[13] R.J. Mata, F. Chérif, Boyd, The Quantum Theory of Atoms in Molecules: From Solid State to DNA and Drug Design, Wiley-VCH, Weinheim, 2007.

[14] P.L.A. Popelier, Atoms in Molecules : An Introduction, Prentice Hall, Harlow, 2000 (etc.).

[15] H.M. Rietveld, A profile refinement method for nuclear and magnetic structures, J. Appl. Crystallogr. 2 (1969) 65–71, http://dx.doi.org/10.1107/S0021889869006558.

[16] A.C. Larson, R.B. Von Dreele, General Structure Analysis System (GSAS) Los Alamos National Laboratory Report LAUR 86-748, 1994.

[17] Brian H. Toby, EXPGUI, a graphical user interface for GSAS, J. Appl. Cryst. 34 (2001) 210–213.

[18] G. Kresse, J. Furthmüller, Efficiency of ab-initio total energy calculations for metals and semiconductors using a plane-wave basis set, Comput. Mater. Sci. 6 (1996) 15–50, http://dx.doi.org/10.1016/0927-0256(96)00008-0.

[19] G. Kresse, J. Hafner, Ab initio molecular-dynamics simulation of the liquid-metal–amorphous-semiconductor transition in germanium, Phys. Rev. B 49 (1994) 14251–14269, http://dx.doi.org/10.1103/PhysRevB.49.14251.

[20] G. Kresse, From ultrasoft pseudopotentials to the projector augmented-wave method, Phys. Rev. B 59 (1999) 1758–1775, http://dx.doi.org/10.1103/PhysRevB.59.1758.

[21] J.P. Perdew, K. Burke, M. Ernzerhof, Generalized gradient approximation made simple, Phys. Rev. Lett. 77 (1996) 3865–3868, http://dx.doi.org/10.1103/PhysRevLett.77.3865.

[22] W. Hohenberg, P. Kohn, Inhomogeneous electron gas, Phys. Rev. 136 (1964) B864–B871, http://dx.doi.org/10.1103/PhysRev.136.B864.

[23] P. Kubelka, Ein Beitrag zur Optik der Farban striche, Zeit Tech. Phys. 12 (1931) 593–603.

[24] A. Escobedo Morales, E. Sánchez Mora, U. Pal, Use of diffuse reflectance spectroscopy for optical characterization of un-supported nanostructures, Rev. Mex. Fis. S 53 (2007) 18–22.

[25] R.L. Carter, Vibrational spectra of Ag_2CrO_4, Spectrosc. Lett. 5 (1972) 401–406, http://dx.doi.org/10.1080/00387017208065408.

[26] D. Santamaría-Pérez, E. Bandiello, D. Errandonea, J. Ruiz-Fuertes, O. Gomis, J. A. Sans, et al., Phase behavior of Ag_2CrO_4 under compression: structural, vibrational, and optical properties, J. Phys. Chem. C 117 (2013) 12239–12248, http://dx.doi.org/10.1021/jp401524s.

[27] R.J.H. Clark, T.J. Dines, Raman, resonance Raman, and infrared spectroscopic study of silver(I) chromate, Inorg. Chem. 21 (1982) 3585–3588, http://dx.doi.org/10.1021/ic00140a002.

Please cite this article as: M.T. Fabbro, et al., J. Solid State Chem. (2016), http://dx.doi.org/10.1016/j.jssc.2016.03.050